Available online at www.sciencedirect.com
SCIENCE DIRECT
Journal of Solid State Chemistry 179 (2006) 2511–2520
JOURNAL OF SOLID STATE CHEMISTRY
www.elsevier.com/locate/jssc

Properties of cerium–zirconium mixed oxides partially substituted by neodymium: Comparison with Zr–Ce–Pr–O ternary oxides

Jana Mikulova, Sylvie Rossignol*, Francois Gérard†, Danielle Mesnard, Charles Kappenstein, Daniel Duprez

Laboratoire de Catalyse en Chimie Organique, UMR 6503, CNRS et Université de Poitiers, 40 Avenue du Recteur Pineau, 86022 Poitiers, France

Received 20 February 2006; received in revised form 6 April 2006; accepted 8 April 2006
Available online 20 May 2006

Abstract

CeO_2 doped with praseodymium, neodymium and/or zirconium atoms were prepared by coprecipitation and by the sol–gel method. Structural properties were investigated by in situ XRD and Raman spectroscopy while oxygen storage capacity (OSC) was measured by transient CO oxidation. All the compounds, except pure Nd_2O_3, have a fluorite-type structure as well as a Raman band at 560 cm^{-1} characteristic of the oxygen vacancies involving non-stoichiometric oxides. The lattice parameter under hydrogen, being dependent on the temperature, revealed two reduction mechanisms: one at a low temperature at the surface and another at a high temperature in the bulk. Ce–Nd binary oxides show a strong tendency towards crystallite aggregation, which reduces accessibility to gases and OSC properties. Zirconium improves the thermal resistance to sintering of both Ce–Nd and Ce–Pr oxides. The Zr–Ce–Pr–O followed by Zr–Ce–Nd–O compounds displaying high oxygen mobility at a low temperature, appear to be very promising for practical applications such as OSC materials.

Keywords: Oxides; Chemical synthesis; Sol–gel chemistry; In situ X-ray diffraction; Oxygen mobility

1. Introduction

Ceria-based materials displaying high oxygen mobility and oxygen storage capacity (OSC) have been extensively investigated due to their wide application in the field of catalysis [1–3]. In the 1990s, many studies were devoted to ZrO_2–CeO_2 oxides, notably to their synthesis and their catalytic properties [4–6]. Nanocrystalline powders of ceria doped with various rare earth cations have been synthesized by coprecipitation using ammonium carbonate as a precipitant [7–10]. Several other mixed oxides Ce–M–O (with M = Eu, Pr, Sm, Nd) were recently investigated with the aim of improving oxygen mobility [11–15]. These oxides were prepared by different ways: (i) Ce–Sm–O oxides by a citrate route [16], (ii) Ce–Eu–O compounds by a hydrothermal route 11, (iii) Ce–Pr–O compounds by coprecipitation 12, and (iv) Ce–Nd–O compounds by the sol–gel method [14]. In many studies, M cations have been used in ternary systems as dopant in Ce–Zr–O mixed oxides.

To characterize the oxygen vacancies due to the aliovalent doping cations, various techniques can be employed, including Raman spectroscopy and in situ XRD studies [17–19]. These aliovalent doping cations, whose valence state is different from that of zirconium ions, preserve the formation of a fluorite-type structure. The range of existence depends on the nature of the cation; for example, the solubility of Sm^{3+} and Nd^{3+} ions is limited to $x = 0.40$ in the $Ce_{1-x}M_xO_2$ system, while that of Pr ions (mainly Pr^{4+}) is limited to $x = 0.75$ in the $Ce_{1-x}Pr_xO_2$ oxides [14,17] Moreover, the thermal expansion coefficient increases with the substitution percentage of the dopant, also creating greater formation of oxygen vacancy. These features may also be confirmed by a Raman band at 560 cm^{-1} mainly ascribed to these oxygen vacancies [20,21].

Previous work on Ce–Pr–O and Zr–Ce–Pr–O mixed oxides, prepared either by the sol–gel method or by

*Corresponding author. Fax: +33 5 49 45 40 20.
E-mail address: Sylvie.rossignol@univ-poitiers.fr (S. Rossignol).
†Deceased.

0022-4596/$ - see front matter © 2006 Elsevier Inc. All rights reserved.
doi:10.1016/j.jssc.2006.04.051

coprecipitation, has shown that the substitution of cerium with praseodymium atoms leads to materials with very high OSC. The simultaneous presence of Pr^{3+} and Pr^{4+} cations, which induce oxygen vacancies, significantly increases oxygen mobility. The purpose of this study is (i) to understand the role played by the substitution of cerium with neodymium cations in CeO_2 and Zr–Ce–O mixed oxides synthesized by coprecipitation or by the sol–gel method and (ii) to compare the behaviour of Nd-containing materials with Zr–Ce–Pr–O oxides. The solids were characterized by in situ powder X-ray diffraction under hydrogen, Raman spectroscopy and BET surface area. OSC was also determined for some samples.

2. Experimental

2.1. Preparation

Two types of oxides were prepared (i) $Ce_{1-x}Nd_xO_2$ by coprecipitation and (ii) $Zr_{0.10}(Ce_{1-x}M_x)_{0.90}O_2$ (M = Pr or Nd) by the sol–gel method previously described [12]. In this work, it was been proved that the use of the sol–gel method for the preparation of Zr-based mixed oxides gives better samples in terms of homogeneity and OSC than coprecipitation. It must be pointed out that only Zr-alkoxides were employed in the preparation while other elements were introduced as nitrates. The relatively low rate of hydrolysis and polycondensation of Zr-alkoxide makes it a very good control of the preparation. To confirm these features two new samples containing zirconium atoms were prepared by coprecipitation using zirconyl and rare-earth nitrate as precursors. However Ce–Nd–O oxides not containing Zr were prepared by the conventional coprecipitation technique. All reactants and solvents were Aldrich products, 99% purity. They were used without any further purification. The amounts of reactants were adjusted so as to obtain 3 g of solid.

2.1.1. Sol–gel method

After being dissolved in 20 cm^3 of isopropyl alcohol (RP, $H_2O \leqslant 0.5\%$), zirconium *n*-propoxide precursor $Zr(OC_3H_7)_4$ (70% in 1-propanol) was slowly added (1 $cm^3\,min^{-1}$, ambient temperature) to an aqueous solution of $Ce(NO_3)_3 \cdot 6H_2O$ and $Pr(NO_3)_3 \cdot 6H_2O$ or $Nd(NO_3)_3 \cdot 6H_2O$ (20 cm^3, stirring speed: 500 rpm). A pseudo-gel formed immediately as the reactant mixture undergone hydrolysis.

2.1.2. Coprecipitation method

Cerium–neodymium oxides were prepared by co-precipitation according to the following procedure. In all, 12 cm^3 of aqueous ammonia (14.7 M) was slowly added to an aqueous solution of zirconyl nitrate or $Ce(NO_3)_3, \cdot 6H_2O$ and $Nd(NO_3)_3 \cdot 6H_2O$ (40 cm^3 in distilled water). The precipitates were filtered, re-dispersed in 100 cm^3 of the ammonia solution (0.25 M) and filtered again.

The samples were dried for 1 h at 333 K in a sand bath and dried for 12 h at 413 K in a ventilated oven and calcined under air for 4 h at 1173 K.

2.2. Characterization

Specific surface areas were determined by N_2 (Air Liquide, 30% N_2 in He) adsorption at 77 K with a Micromeritics Flow Sorb II.

Structure and crystallite sizes were determined by X-ray diffraction carried out on a Siemens D 5005 powder θ–θ diffractometer using the Cu$K\alpha$ radiation ($\lambda_{K\alpha}$ = 0.15418 nm) and a secondary graphite back monochromator. The diffractograms were obtained under the following conditions: dwell time: 2 s; step: 0.04° 2θ; divergence slit: 1°. The crystalline phases were identified by comparison with ICDD standards. In situ X-ray measurements were carried out in a HTK16 high-temperature stainless steel chamber linked to a D500 diffractometer. The diffractograms were recorded by increments of 0.028° with a dwell time of 10 s. The powdered oxides (about 20 mg) were suspended in ethanol and deposited as a thin layer on a Kanthal foil which supported the sample and heated by the Joule effect. The oxides were heated under air or hydrogen from 298 to 1273 K at a heating rate of 0.10 $K\,s^{-1}$. They were subsequently cooled down at 0.16 $K\,s^{-1}$ (normal cooling) or at $\approx 3\,K\,s^{-1}$ (quenching mode) in the presence of hydrogen.

Raman spectra were collected using a Perkin Elmer spectrometer equipped with an Nd-YAG laser (1064.4 nm). Experimental conditions were: laser power = 100 mW, acquisition time = 120 s, number of scans = 20 and resolution = 4 cm^{-1}. For FT-IR spectra, the same apparatus was used but in IR mode.

OSC was measured at 673 and 773 K under atmospheric pressure. A 20 mg sample was continuously purged with helium (30 $cm^3\,min^{-1}$). Alternate pulses (0.265 cm^3) of O_2 (Air Liquide, $\leqslant 5$ ppm total impurities) and CO (Air Liquide) were injected every minute in order to simulate lean and rich operating conditions such as those encountered in an Otto engine coupled with a three-way catalytic converter. The OSC was calculated from CO consumption or CO_2 formation after the first CO pulse.

3. Results

3.1. Oxygen deficiency of the compounds

The chemistry of neodymium mainly in its +III oxidation state leads to materials with an oxygen content which takes into account the simultaneous presence of Ce^{4+}, Ce^{3+} and Nd^{3+} ions generating oxygen defect ($(O/Ce + Nd) < 2$). Consequently, the Ce–Nd–O samples should be written $Ce_{1-x}Nd_xO_{2-\xi}$. Let a be the fraction of Ce^{3+} in the $(1-x)$ cerium ions. If all the neodymium ions are in the +III oxidation state, then $\xi = 0.5\,[x + a(1-x)]$. It can be verified that $\xi = 0.5$ for $x = 1$ (pure Nd oxide) and

$\xi = 0.5a$ for $x = 0$ (pure ceria). The previous formula can also be written as $Ce_{1-x}Nd_xO_{2-0.5x-\delta}$ with $\delta = 0.5a\,(1-x)$. For instance, the solid with $x = 0.5$ is $Ce_{0.5}Nd_{0.5}O_{1.75-\delta}$ with $\delta = 0.25a$.

For the same reason, the ternary oxides (CP or SG) should be written $Zr_{0.10}(Ce_{0.75}M_{0.25})_{0.90}O_{2-\xi}$ (M = Nd or Pr). Let a be the fraction of Ce^{3+} in the 0.675 cerium ions. For the neodymium compound, $\xi = 0.1125 + 0.3375a$ and its approximated formula is $Zr_{0.10}(Ce_{0.75}M_{0.25})_{0.90}O_{1.89-\delta}$ with $\delta = 0.337a$. For the praseodymium compound, both Ce and Pr may have two oxidation states: +III and +IV. If b is the faction of Pr^{3+} in the 0.225 praseodymium ions, then $\xi = 0.3375a + 0.1125b$.

3.2. Structural data: XRD at ambient temperatures

Nomenclature and characteristics of the binary Ce–Nd–O and the ternary Zr–Ce–Pr–O or Zr–Ce–Nd–O oxides are listed in Table 1. The colour of Ce–Nd–O mixed oxides changes from yellow for cerium oxide to purple for the neodymium oxide. Substitution of cerium with neodymium atoms in ceria does not improve the thermal stability: BET values are very small, in the range of a few $m^2\,g^{-1}$. In the presence of zirconium atoms, a significant improvement of the BET surface area values can be observed which is emphasized with sol–gel samples [22]. For the same preparation procedure, the addition of neodymium or praseodymium cations in the Zr–Ce–O oxides gives a very similar BET area [17], which suggests that the high stability of Zr–Ce oxides are virtually not affected by the presence of these rare earth elements. On the contrary, for the same sample prepared by the sol–gel or coprecipitation mode, the difference observed agrees with results observed in previous work [12].

Fig. 1 shows the room temperature XRD patterns of $Ce_{1-x}Nd_xO_{2-\xi}$ oxides calcined at 1173 K. Single oxides have been indexed respectively by the ICCD files 34-0394 for CeO_2 and 41-1089 for Nd_2O_3. In previous studies on Pr-promoted Ce–Zr–O oxides, the Pr_6O_{11} sub-oxide was clearly identified in pure praseodymium oxide [17]. Contrary to PrO_x, neodymium sub-oxide (such as Nd_6O_{11}) is not detected, which gives evidence that only Nd^{3+} ions are present instead of a mixture of Nd^{3+}/Nd^{4+}. As it was already observed with Ce–Pr–O oxides, the Ce-rich sample ($Ce_{0.75}Nd_{0.25}O_{1.88-\delta}$) displays a solid solution with a fluorite-type structure. For the other compounds ($Ce_{1-x}Nd_xO_2$, $x = 0.50$ and 0.75), the highest peaks can be attributed to both the fluorite-type structure and Nd_2O_3 phase. Consequently, the formation of a pure crystallographic phase seems limited to $x = 0.25$ in the $Ce_{1-x}Nd_xO_{2-\xi}$ oxide series. In the $Ce_{1-x}Pr_xO_{2-\xi}$ system, no phase demixion was observed and pure solid solutions could be obtained up to $x = 0.75$. For other Ce–M–O systems with M = Eu or Sm, the domain of existence of the solid solution seemed limited to $x = 0.40$ [11,13]. For the two preparation procedures (CP or SG), in the

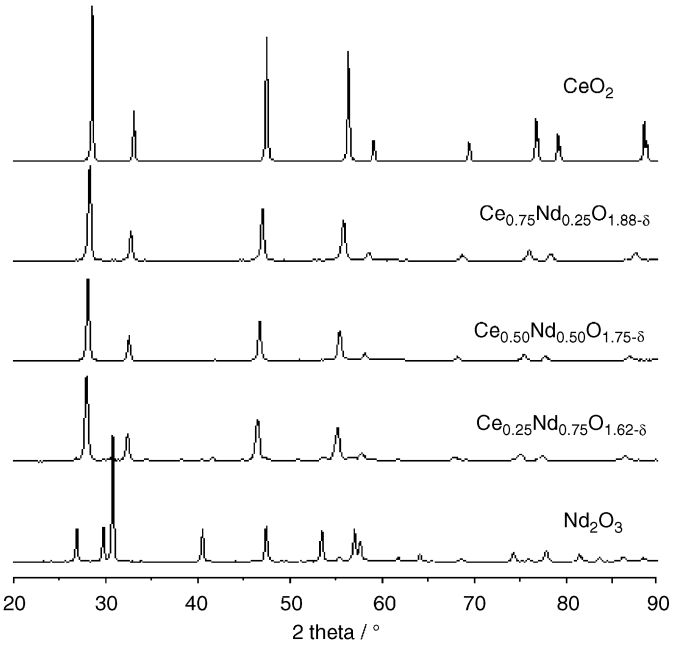

Fig. 1. Room temperature X-ray pattern of Ce–Nd–O compounds calcined at 1173 K (ICCD files 34-0394 for CeO_2 and 41-1089 for Nd_2O_3).

Table 1
Colour, oxygen storage capacity values, BET area and crystallite size for various samples calcined at 1173 K

Samples	Colour	BET area $m^2\,g^{-1}$	OSC μmol at .0 g^{-1}		Lattice parameter (nm)	Crystallite size (nm)
			673 K	773 K		
Nd_2O_3	Purple	<1	2			70
$Ce_{0.25}Nd_{0.75}O_{1.62-\delta}$	Grey	3	5		0.5528	42*
$Ce_{0.50}Nd_{0.50}O_{1.75-\delta}$	Olive green	4	15		0.5494	53*
$Ce_{0.75}Nd_{0.25}O_{1.88-\delta}$	Almond	5	17		0.5459	45
$CeO_{2-\xi}$	Yellow	3	78		0.5411	70
$^{SG}Zr_{0.10}(Ce_{0.75}Nd_{0.25})_{0.90}O_{1.89-\delta}$	Straw-coloured	28	107	125	0.5415	30
$^{SG}Zr_{0.10}(Ce_{0.75}Pr_{0.25})_{0.90}O_{2-\xi}$	Crimson	26	117	275	0.5422	40
$^{CP}Zr_{0.10}(Ce_{0.75}Nd_{0.25})_{0.90}O_{1.89-\delta}$	Straw-coloured	6		79	0.5417	28
$^{CP}Zr_{0.10}(Ce_{0.75}Pr_{0.25})_{0.90}O_{2-\xi}$	Crimson	10		188	0.5423	30

*Phase mixture, SG: sol–gel, CP: coprecipitation.

$Zr_{0.10}(Ce_{0.75}M_{0.25})_{0.90}O_{2-\xi}$ (M = Nd or Pr) ternary oxides, a pure fluorite-like phase was observed (X-ray patterns not shown).

At room temperature, the substitution of cerium with neodymium atoms causes the lattice parameter to increase. The addition of Zr atoms in the ternary mixtures causes the lattice to decrease. This feature is less pronounced in the presence of praseodymium atoms in which Pr may be at the two oxidation states Pr^{4+} and Pr^{3+}. The increase of lattice parameter in Zr–Ce–Pr–O with respect to Zr–Ce–Nd–O suggests (i) the presence of Pr^{4+}–Pr^{3+} ions and (ii), that the greater radius of Pr^{3+} ions determines the final cell volume in the cubic structure. This variation of lattice parameter will be discussed in term of ionic radius and valence state (see paragraph 2 of Section 4).

The crystallite size determined by XRD (Table 1) is larger in single oxides than in mixed oxides. For binary or ternary oxides, these values crystallite size agree well with the values found for other mixed oxides [13], and are characteristic of less crystallized materials. This may be due to a disorder induced by Pr^{4+}/Pr^{3+} and Nd^{3+} aliovalent cations.

3.3. Structural data: Raman spectroscopy

The Raman spectrum of CeO_2 (Fig. 2) shows only the band at 464 cm^{-1} attributed to the T_{2g} mode in the $Fm3m$ space group [23]. The bands at 270 and 315 cm^{-1}, characteristic of small crystallites (4 nm or less) are not observed, which agree with the crystallite size calculated by X-ray line broadening [20]. For the Nd_2O_3 compound, all the Raman shift bands (0–1000 cm^{-1}) can be attributed to the A-type structure (space group P_{3m1}) [24]. The Raman spectrum of the $Ce_{0.75}Nd_{0.25}O_{1.88-\delta}$ sample mainly consists of two bands: one at 464 cm^{-1} ascribed to the fluorite-type structure which agrees with XRD data, and another at 560 cm^{-1}. The latter last has been attributed to the presence of oxygen vacancies in the fluorite-type structure and may indicative of significant oxygen mobility in this solid [25]. The Raman spectra of the $Ce_{0.50}Nd_{0.50}O_{1.75-\delta}$ and $Ce_{0.25}Nd_{0.75}O_{1.62-\delta}$ samples show features characteristic of a phase mixture of Nd_2O_3 and mixed oxide with a fluorite-type structure (band at 464 cm^{-1}) which agrees with XRD data. Whatever the rare-earths (Nd or Pr) atoms, the Raman spectra of $Zr_{0.10}(Ce_{0.75}M_{0.75})_{0.90}O_2$ sol–gel and coprecipated samples consist of two main bands at 464 and 560 cm^{-1} (Fig. 3a), which confirm the presence of a fluorite-type structure; even the band at 560 cm^{-1} is more pronounced for compounds containing praseodymium cations. With a weak amount of zirconium, the preparation mode results in compounds with similar structural data.

In order to confirm the presence of these bands, one experiment recorded at another excitation line ($\lambda = 525$ nm) was performed on the $^{SG}Zr_{0.10}(Ce_{0.75}Nd_{0.75})_{0.90}O_{1.89-\delta}$ compound (Fig. 3b). The main bands at 464 and 560 cm^{-1} are invariant when the frequency of the excitation line is changed and they may definitively be ascribed to the fluorite structure and oxygen vacancies, exactly as it was for the spectra recorded at $\lambda = 1064.4$ nm. To overcome possible ambiguities in the structural information extracted from the Raman spectra, at least two laser excitation lines must be used as described by Fornasiero et al. [26]. All these results show that compounds based on praseodymium or neodymium cations display the same structural features with respect to oxygen vacancies. This would suggest that the solids can possess relatively high oxygen mobility.

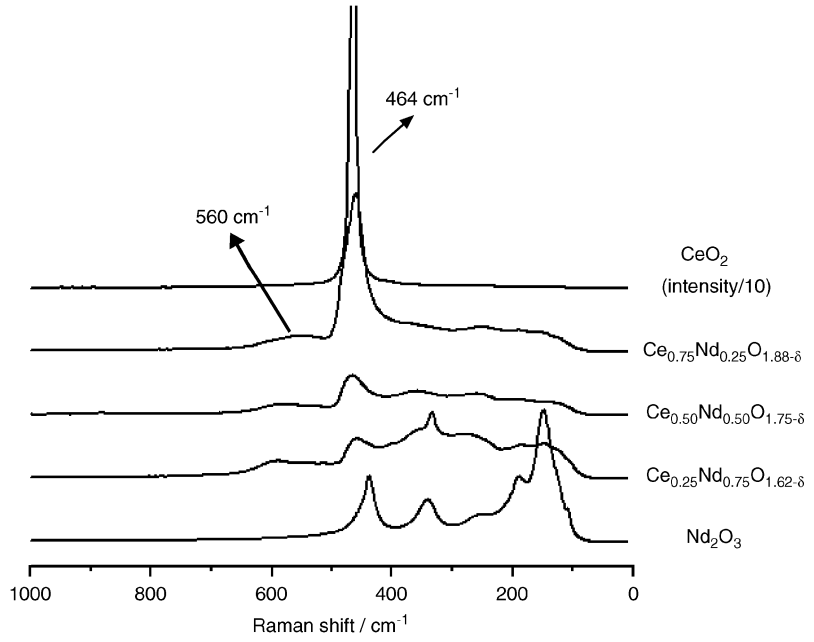

Fig. 2. Room temperature Raman spectra of Ce–Nd–O compounds under air atmosphere.

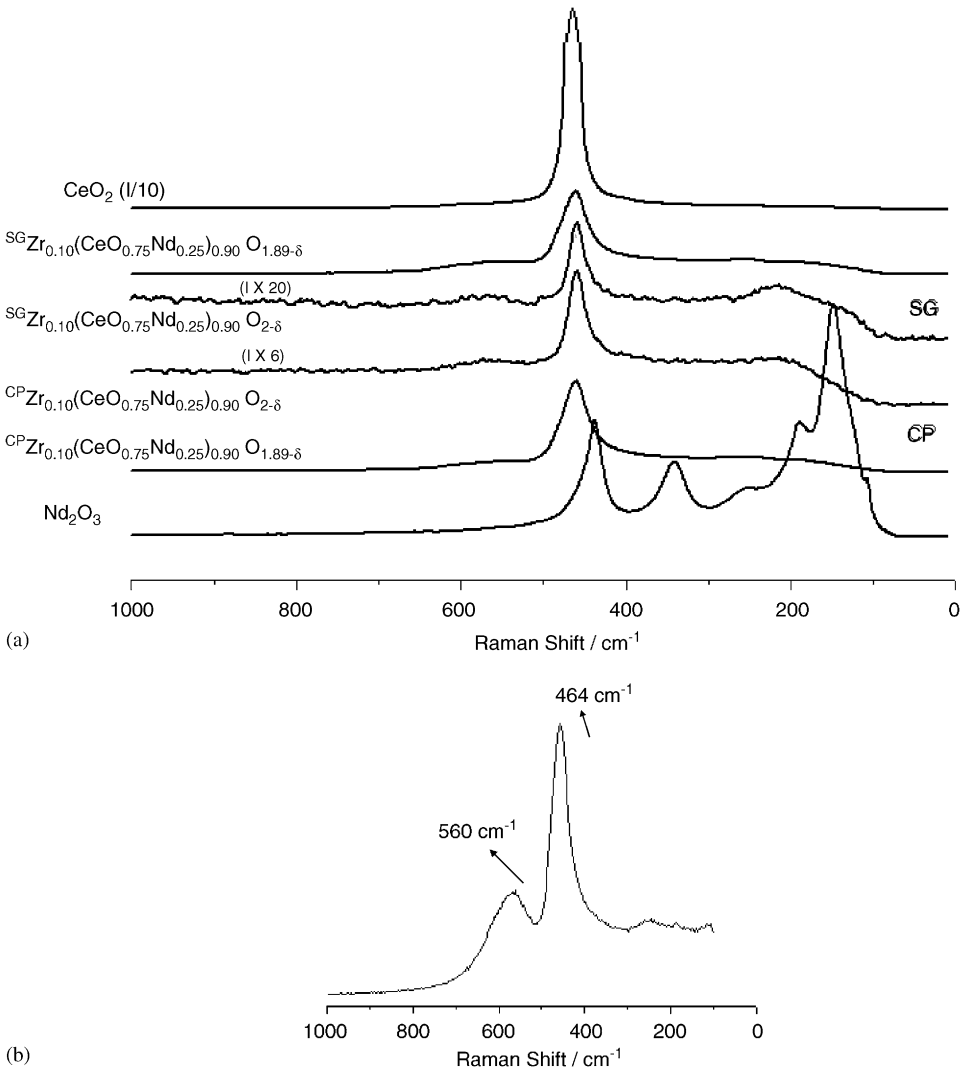

Fig. 3. (a) Raman spectra of $Zr_{0.10}(Ce_{0.75}M_{0.25})_{0.90}O_{2-\xi}$ (M = Pr or Nd), CeO_2 and Nd_2O_3 compounds under air at room temperature ($\lambda = 1064.4$ nm), (b) Raman spectrum of $^{SG}Zr_{0.10}(Ce_{0.75}Nd_{0.25})_{0.90}O_{1.89-\delta}$ sample ($\lambda = 525$ nm).

3.4. In situ XRD studies

Several samples displaying a solid solution (fluorite-type structure) were further investigated by in situ XRD, which allowed the lattice parameter at temperatures ranging from 298 to 1273 K to be determined. The results obtained for the $Ce_{0.75}Nd_{0.25}O_{1.88-\delta}$ sample under air or hydrogen are reported in Fig. 4.

In an oxidizing atmosphere, this sample shows unique thermal behaviour over the entire range of temperatures. The thermal expansion coefficient ($\alpha_T = 1.27 \times 10^{-5}\,K^{-1}$) is close to that of pure ceria or that of $Ce_{0.90}Zr_{0.10}O_2$ ($\alpha_T = 1.24 \times 10^{-5}\,K^{-1}$) and slightly lower than that of $Ce_{0.70}Pr_{0.30}O_2$ ($2.53 \times 10^{-5}\,K^{-1}$) in previous studies [17]. Indeed, in this latter compound, several oxygen vacancies are in evidence at room temperature, predicting more significant oxygen mobility. Consequently, weak oxygen mobility is suspected in Ce–Nd–O oxide whose thermal

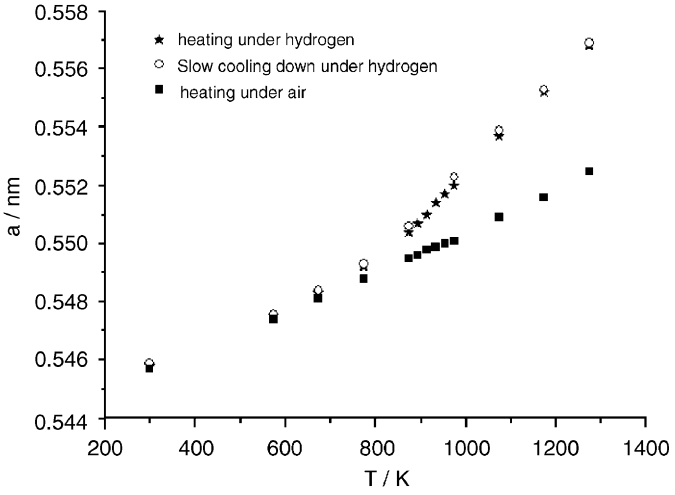

Fig. 4. Temperature dependence of the lattice parameter under air or hydrogen atmosphere for the $Ce_{0.75}Nd_{0.25}O_{1.88-\delta}$ compound.

expansion coefficient is close to that of ceria. These results show that the rare earth-mixed oxides under study exhibit very similar behaviour under air with a linear increase of the lattice parameter over the entire range of temperatures [17].

In a reducing atmosphere, two temperature ranges can be observed for the variation of lattice parameter with an inflexion point at about 700 K (Fig. 4). There is no hysteresis in this expansion phenomenon. The same behaviour with the same slope can also be observed upon slow cooling in H_2. From 298 to 700 K, the changes of lattice parameter are very similar in air and in H_2 and may be ascribed to a mere thermal expansion of the lattice. Above 700 K the lattice parameter increases more rapidly in H_2 than in air. This feature can be attributed to a bulk reduction of the compound (Ce^{4+} into Ce^{3+}) which applies to the thermal linear expansion of the cell.

The temperature dependence of the lattice parameter in a hydrogen atmosphere is shown in Fig. 5, for the three compounds as well as for pure ceria. Whatever the mixed oxide, the same behaviour can be observed: (i) at low temperatures, there is a linear thermal expansion close to that of ceria and (ii) at high temperatures, an increase of the thermal expansion coefficient is observed, which is characteristic of sample reduction with the formation of anionic vacancies [17] The transitional temperatures between the two dilatation regimes (A–C in Fig. 5) depend on the nature of the oxide and vary from 580 K for $Zr_{0.10}(Ce_{0.75}Pr_{0.25})_{0.90}O_{2-\xi}$ (B) to 670 K for $Zr_{0.10}(Ce_{0.75}Nd_{0.25})_{0.90}O_{1.89-\delta}$ (A) and 780 K for $Ce_{0.75}Nd_{0.25}O_{1.88-\delta}$ (C). These reduction steps occurred at relatively different temperatures, which emphasize the role played by the rare earth element added to Ce and Zr (ionic radius, possibility of various oxidation states). However, the behaviour of the binary and ternary oxides contrasts with that of pure ceria. Whereas CeO_2 exhibits a sharp increase of its lattice parameter between 900 and 1000 K, there is a smoother transition for the mixed oxides. It seems as if the bulk reduction in the binary and ternary oxides starts at lower temperatures and much more gradually than in pure ceria. The materials displaying the lowest transition temperature should possess the highest oxygen mobility in the bulk. This was tentatively verified by measuring the oxygen storage capacities of the mixed oxides.

3.5. Oxygen storage capacity

3.5.1. Fast oxygen storage (first pulse)

The comparison of in situ XRD data with OSC values would have required that storage experiments be carried out with H_2 as reducing gas. Carbon monoxide was however chosen for the following reasons: (i) CO is currently used in most OSC measurements [27–30] and (ii) there are many similarities between OSC(CO) and OSC(H_2) [29]. Moreover, it has been demonstrated that CO is a more effective reducing agent than H_2 for mixed oxide. The same results were observed with TPR measurements [31]. Some works have been performed with H_2-OSC and reveal the complexity of this mechanism and highlight the necessity of comparing both interactions of CO and of H_2 with material surfaces [32].

As a rule, two mechanisms can account for oxygen storage in oxide materials: (i) either there is diffusion of oxygen species from the bulk to the surface and the reaction with the reducer (H_2 or CO) takes place at the surface or (ii) the reaction takes place in the bulk, which implies that there is bulk diffusion of the reducer and back-diffusion of the reaction products (H_2O or CO_2). The second mechanism is quite unlikely for OSC(CO) while it cannot be excluded for OSC(H_2): hybrid species have been

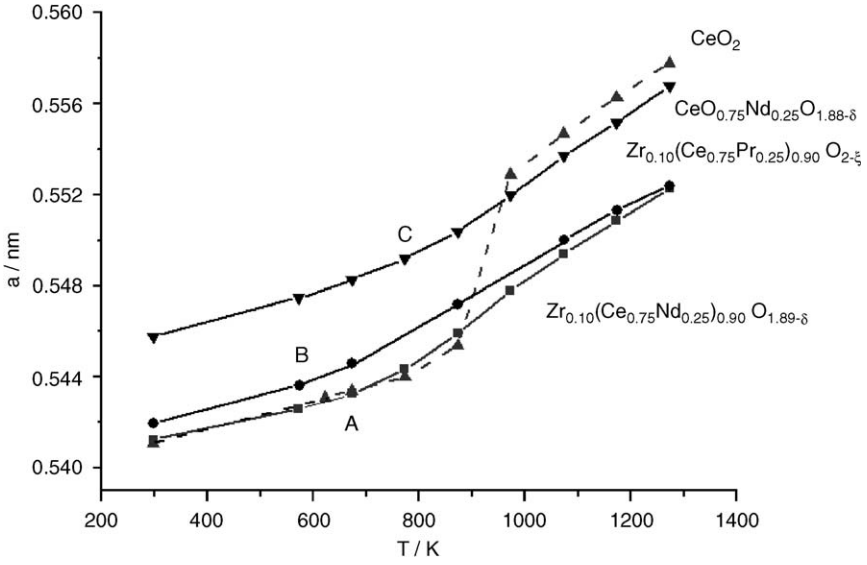

Fig. 5. Temperature dependence of the lattice parameter under hydrogen for the mixed oxides (A: $Zr_{0.10}(Ce_{0.75}Nd_{0.25})_{0.90}O_{1.89-\delta}$; B:$Zr_{0.10}(Ce_{0.75}Pr_{0.25})_{0.90}O_{2-\xi}$; C: $Ce_{0.75}Nd_{0.25}O_{1.88-\delta}$).

observed with the reaction of rare earth oxides with hydrogen [18] and the back-diffusion of water via hydroxyl groups is a common phenomenon in oxide dehydration. In summary, OSC(CO) is mainly controlled by oxygen mobility while more complex mechanisms can occur as long as OSC(H_2) is concerned.

OSC expressed in μmol at. O g^{-1} for the different samples measured at 663 K are reported in Table 1. Substituting cerium with neodymium cations in ceria decreases oxygen mobility, which can be ascribed to the unique oxidation state (+III) of neodymium in these compounds. The +III neodymium cation has a negative effect on Ce reduction and the redox process is virtually suppressed despite the oxygen vacancies observed by Raman spectroscopy. On the contrary, replacing cerium with praseodymium cations increases oxygen mobility owing to the presence of both Pr^{4+} and Pr^{3+} cations [12].

Whatever samples to which zirconium is added, the Ce–Nd–O stabilizes the structure and enhances oxygen mobility [33]. However, the preparation mode results in clear differences, sol–gel samples being better than coprecipitated samples [22]. Remarkably, Zr^{4+} restores OSC properties of Ce–Nd oxides. The very different values obtained at 773 K for the two materials containing the same amounts of zirconium and cerium atoms are obviously linked to the nature of the second rare earth element. Praseodymium ability is to rapidly change its oxidation state seems to favour a greater reduction of Ce^{4+} into Ce^{3+} and to improve oxygen mobility.

3.5.2. *Oxygen storage capacity complete (OSCC, 10 pulses at 773 K)*

In order to give a better overview of the redox process in the ternary oxides, the experimental data obtained at 773 K in all experiments (10 pulses of CO, then 10 pulses of O_2, and finally alternate pulses of CO and O_2) are reported in Table 2 for $Zr_{0.10}(Ce_{0.75}Pr_{0.25})_{0.90}O_{2-\xi}$ and in Table 3 for the $Zr_{0.10}(Ce_{0.75}Nd_{0.25})_{0.90}O_{1.89-\delta}$ solid. With the ternary Zr–Ce–Pr oxide, the amount of CO_2 produced after the first pulse of CO exactly matches with the amount of CO consumed. In the following pulses, some carbon seems to be trapped on or in the materials with a cumulated deficit of CO_2 formed with respect to the CO consumed. Nevertheless, this left over carbon is not totally eliminated during oxidation treatment. Some amount of CO can be stored on the surface in a non-oxidized form (e.g. formates), which can be oxidized into carbonaceous species during O pulses. Consequently these species do not leave the surface and no CO_2 is produced. After alternate pulses of CO and O_2, CO_2 production and CO consumption agree well. Furthermore, the O_2 uptake corresponds to a complete re-oxidation of the surface [Eqs. (1) and (2)]:

$$CO_{(g)} + 2CeO_2(s) \rightarrow 2CeO_{2-\xi}(s) + 2\xi CO_{2(g)}, \quad (1)$$

$$2CeO_{2-\xi}\ (s) + \xi O_2 \rightarrow +2CeO_2(s). \quad (2)$$

Table 2
OSC measurements at 773 K over $^{SG}Zr_{0.10}(Ce_{0.75}Pr_{0.25})_{0.90}O_{2-\xi}$ (sample weight: 20 mg; pulses of 12 μmol of gas)

Pulse number	Treatment under CO		Treatment under O_2	
	CO consumed (μmol g^{-1})	CO_2 formed (μmol g^{-1})	O atoms consumed (μmol g^{-1})	CO_2 formed (μmol g^{-1})
Step 1: 10 pulses CO followed by 10 pulses O_2				
1	274	274	622	0
2	201	197	15	0
3	64	52	4	0
4	31	19	8	0
5	18	0	11	0
6	17	0	0	0
7	15	0	0	0
8	12	0	0	0
9	13	0	0	0
10	11	0	0	0
Total	656	542	660	0
Step 2: Alternate pulses of CO and O_2 (3 pulses of each gas)				
1	275	268	312	0
2	273	272	298	0
3	274	276	296	0

Table 3
OSC measurements at 773 K over $^{SG}Zr_{0.10}(Ce_{0.75}Nd_{0.25})_{0.90}O_{1.89-\delta}$ (sample weight: 20 mg; pulses of 12 μmol of gas).

Pulse number	Treatment under CO		Treatment under O_2	
	CO consumed (μmol g^{-1})	CO_2 formed (μmol g^{-1})	O atoms consumed (μmol g^{-1})	CO_2 formed (μmol g^{-1})
Step 1: 10 pulses CO followed by 10 pulses O_2				
1	88	79	100	0
2	23	21	17	0
3	14	0	12	0
4	6	0	11	0
5	6	0	10	0
6	6	0	2	0
7	1	0	0	0
8	0	0	0	0
9	0	0	0	0
10	0	0	0	0
Total	144	100	150	0
Step 2: Alternate pulses of CO and O_2 (3 pulses of each gas)				
1	94	76	100	0
2	94	77	103	0
3	95	78	104	0

The non-stoichiometric phase $2CeO_{2-\delta}$ (s) is better described as [12]:

$$[Ce^{IV}_{1-2\xi}Ce^{III}_{2\xi}][O_{2-\xi}(V^{\circ\circ}_O)_\xi], \quad (3)$$

where $V^{\circ\circ}_O$ represent oxygen vacancies.

Contrasting with the Pr-containing oxide, the $Zr_{0.10}(Ce_{0.75}Nd_{0.25})_{0.90}O_{1.89-\delta}$ solid shows unusual oxygen

storage behaviour with the CO consumption being much higher than the CO_2 production between the second and the tenth pulse (Table 3). A likely explanation is that the solid can store a great amount of carbonates not desorbed after oxygen pulses. During the alternate pulses of CO and O_2, similar behaviour is noticed although it is less pronounced. This fact emphasizes the relatively low OSC and the great affinity with respect to CO_2 of the $Zr_{0.10}(Ce_{0.75}Nd_{0.25})_{0.90}O_{1.89-\delta}$ ternary oxide. Neodymium seems to have a negative impact on Ce^{4+} reduction (Fig. 5) and oxygen storage would in part be inhibited by too great an amount of carbonates stored in the solid.

This phenomenon is not so pronounced at 673 K, which explains why the differences in OSC between the two ternary oxides are much smaller at this temperature

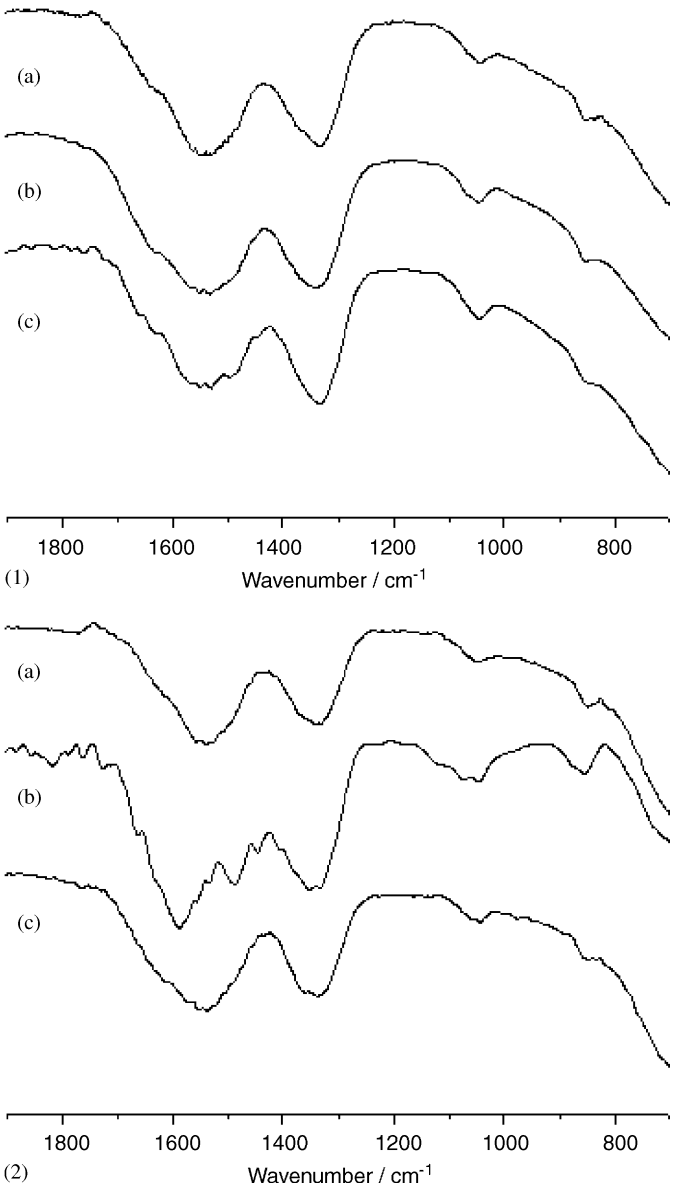

Fig. 6. Room temperature infrared spectra of $^{SG}Zr_{0.10}(Ce_{0.75}M_{0.25})_{0.90}O_{2-\xi}$ (M = Nd (1) or Pr (2)) compounds (a) fresh sample, (b) under CO_2 (1 h; 723 K) and (c) under air (1 h; 723 K).

(Table 1). In summary, $Zr_{0.10}(Ce_{0.75}Pr_{0.25})_{0.90}O_{2-\xi}$ is the sample displaying the highest OSC values in the 673–773 K temperature range.

To prove the existence of carbonates on the surface, some infrared experiments were performed under CO_2 and O_2 at 723 K for the two compounds ($Zr_{0.10}(Ce_{0.75}Pr_{0.25})_{0.90}O_{2-\xi}$ and $Zr_{0.10}(Ce_{0.75}Nd_{0.25})_{0.90}O_{1.89-\delta}$). The procedure followed for the experiments is: recording of (a) spectrum corresponding to the fresh sample; recording of (b) spectrum with the sample treated under CO_2 at 723 K for 1 h and then (c), recording of spectrum corresponding to the last sample heated under air in the same conditions (Fig. 6). Whatever the samples, (a) and (c) spectra are identical and the bands can be attributed to bidentate and monodentate carbonate bands, respectively at 1567, 1289, 1014, 856 and 1504, 1351 cm^{-1} [34]. In the presence of praseodymium cation, treatment under CO_2 results in the formation of additional bands attributed to polydentate and bridged carbonate species (1462, 1353, 1066, 854 and 1736, 1135 cm^{-1}). This modification shows that this compound is able to form various carbonate species while for neodymium compounds the carbonates remain the same on the surface. It seems that some carbonate species can inhibit on the oxygen mobility especially in Nd-containing compounds.

4. Discussion

4.1. Catalyst morphology

The crystallite size deduced from XRD peak broadening allows to calculate the surface area A_{XRD} of the solid. Assuming a spherical shape of these crystallites, one has

$$A_{XRD}(m^2\,g^{-1}) = \frac{6}{\rho d}. \quad (4)$$

ρ being the volumic weight of the solid ($g\,m^{-3}$) and d, the particle size (m). For Nd_2O_3, the volumic weight is $7.24 \times 10^6\,g\,m^{-3}$. For the other oxides having a fluorite-like structure, the volumic weight can be calculated by

$$\rho = \frac{4M}{Na^3}. \quad (5)$$

M being the molar weight of oxide ($g\,mol^{-1}$), N, the Avogadro number ($at.\,mol^{-1}$) and a, the cell parameter (m).

The surface area of the oxides can also be deduced from OSC measurements [17]. For those oxides having very low bulk oxygen mobility, the reduction process is limited to the surface and can be a good means of measuring this surface area assuming an ideal surface. If bulk oxygen mobility is very high, the calculated surface area will be higher than the actual surface area. For the oxides having a fluorite-type structure, there are 4 oxygen atoms per a^2. In ceria, the number of surface oxide ions is close to 13.6 at O nm^{-2}. Assuming that one oxygen atom out of four is available for the OSC process (reduction of Ce^{4+} in

Ce^{3+}), the intrinsic OSC of ceria amounts to 5.67 μmol O m^{-2}. In binary and ternary oxides, only Ce^{4+} and Pr^{4+} can be reduced into trivalent cations consequently intrinsic OSC values (OSC_{int}) should be normalized with respect to these cations. If one assumes that the surface density of the cation is close of that of the bulk (no surface enrichment), the OSCint value for binary $Ce_xNd_{1-x}O_2$ oxides would be $OSC_{int} = N_0(x/4)$ where N_0 is the surface density of O atoms. For $Zr_{0.10}(Ce_{0.75}Pr_{0.25})_{0.90}O_{2-\xi}$, intrinsic OSC would be OSCint = $N_0(0.9/4)$ ($0.9 = Ce^{4+}/Ce^{3+}$ and Pr^{4+}/Pr^{3+}) while for $Zr_{0.10}(Ce_{0.75}Nd_{0.25})_{0.90}O_{1.89-\delta}$, one should have OSCint = $N_0(0.9 \times 0.75/4)$ ($0.75 = Ce^{4+}/Ce^{3+}$; no contribution of Nd^{3+}). The theoretical surface area A_{OSC} accessible to oxygen storage is

$$A_{OSC}(m^2g^{-1}) = \frac{OSC(\mu mol\, g^{-1})}{OSCint(\mu mol\, m^{-2})}. \quad (6)$$

BET surface area and surface area A_{XRD} and A_{OSC} are compared in Table 4. The three measurements of surface area for ceria and ternary oxides agree well, while A_{XRD} is much higher than A_{BET} and A_{OSC} for binary Ce–Nd oxides. In every case, A_{OSC} is close to A_{BET}. These results may be interpreted as follows: in ceria and ternary oxides, elementary grains of oxide are constituted of nanocrystals that virtually have no defects, also corroborated by XRD measurements, corresponding to grains entirely accessible to gases and the oxygen mobility is improved. On the contrary, Ce–Nd oxides present crystals which can be agglomerated and contain many defects. Consequently, the grain boundaries for the most part are not accessible to gases and are responsible for the non-migration of oxygen atoms resulting in weak OSC.

4.2. Variation of the lattice parameter

The calculated value agrees with the work of Li et al. [14]. Kim [35] and Mogensen [36] have reported a general expression of the Vegard's slope. For ceria-based mixed oxides, the variation of the lattice parameter is

$$\Delta a = \sum (0.0220\Delta r_k + 0.00015\Delta z_k)m_k, \quad (7)$$

where Δr_k is the difference in ionic radius ($r_k - r_{Ce}$), Δz_k, the valence difference ($z_k - 4$), and m_k the molar percentage of the kth dopant. Another expression was derived by Hong and Virkar [37] for ceria doped with trivalent elements:

$$\Delta a = 0.023027 \sum (r_k - 0.1024)m_k. \quad (8)$$

The theoretical values calculated by Eq. (7) for the binary and ternary oxides and by Eq. (8) for Ce–Nd oxides are compared with experimental values in Table 5. For binary oxides, a high correspondence can be observed, even though the difference between theoretical and experimental values slightly increases with the neodymium content. This can be ascribed to the fact that $Ce_{0.50}Nd_{0.50}O_{1.75-\delta}$ and particularly $Ce_{0.25}Nd_{0.75}O_{1.62-\delta}$ are not pure crystallographic phases and contain some amounts of neodymium oxide. The relative discrepancy noticed with the ternary oxides may be attributed to the uncertainty of the

Table 4
Comparison of the surface areas of the different oxides determined by N_2 adsorption at 77 K (A_{BET}), by XRD (A_{XRD}, Eq. (4)) and by oxygen storage (A_{OSC}, Eq. (6)).

Oxides	A_{BET} ($m^2 g^{-1}$)	OSC@673 K (μmol O g^{-1})	OSC_{int} (μmol O m^{-2})	A_{OSC} ($m^2 g^{-1}$)	ρ (g cm^{-})	A_{XRD} ($m^2 g^{-1}$)
Nd_2O_3	<1	2	—	—	7.24	11.8
$Ce_{0.25}Nd_{0.75}O_{1.62-\delta}$	3	5	1.39	3.6	6.89	20.7
$Ce_{0.50}Nd_{0.50}O_{1.75-\delta}$	5	15	2.79	5.4	6.97	16.2
$Ce_{0.75}Nd_{0.25}O_{1.88-\delta}$	4	17	4.18	4.1	7.07	18.9
$CeO_{2-\xi}$	10	78	5.67	13.7	7.21	11.9
$^{SG}Zr_{0.10}(Ce_{0.75}Nd_{0.25})_{0.90}O_{1.89-\delta}$	28	107	3.83	28.0	7.03	28.4
$^{SG}Zr_{0.10}(Ce_{0.75}Pr_{0.25})_{0.90}O_{2-\xi}$	26	117	5.09	23.0	6.97	21.5

Table 5
Variation of the lattice parameter in binary and ternary oxides (fluorite structure) with respect to that of pure ceria. Comparison between experimental values and theoretical values given by Eq. (7) (Kim[31]) or Eq. (8) (Hong and Virkar[33]).

Oxide	Δa (nm) experimental	Δa (nm) Eq. (7)*	Δa (nm) Eq. (8)*
$Ce_{0.25}Nd_{0.75}O_{1.62-\delta}$	0.0117	0.0135	0.0166
$Ce_{0.50}Nd_{0.50}O_{1.75-\delta}$	0.0083	0.0090	0.0111
$Ce_{0.75}Nd_{0.25}O_{1.88-\delta}$	0.0048	0.0045	0.0055
$^{SG}Zr_{0.10}(Ce_{0.75}Nd_{0.25})_{0.90}O_{1.89-\delta}$	0.0004	0.0016	—
$^{SG}Zr_{0.10}(Ce_{0.75}Pr_{0.25})_{0.90}O_{2-\xi}$	0.0011	0.0021 (Pr^{3+}) −0.0014 (Pr^{4+})	—

*r_k values (nm) taken for the calculation: Zr^{4+}, 0.086; Ce^{4+}, 0.097; Nd^{3+}, 0.112; Pr^{4+}, 0.099 and Pr^{3+}, 0.113.

predictive equation for such small Δa values. However, the same tendency between theoretical and experimental values is observed, which confirms that Eq. (7) can be used for the estimation of Vegard's slopes in complex oxides. The behaviour of the ZrCePr ternary oxide is also worthy of note: while the calculation with Pr^{4+} cations gives negative Δa values, only those obtained with Pr^{3+} cations lead to positive values agreeing with experimental data. Most likely, Pr ions are present as trivalent and tetravalent doping in this ternary oxide. This feature, as well as the temperature dependence of the Pr-containing oxides (Fig. 5 and Ref. [17]) illustrates the difference between Ce doping with Pr or with Nd.

5. Conclusion

Binary Ce–Nd and ternary Zr–Ce–Nd and Zr–Ce–Pr oxides were prepared by the sol–gel method and calcined at 1173 K. The binary Ce–Nd oxides are characterized by a solid solution with a fluorite-type structure until $x = 0.25$ and by relatively weak oxygen mobility, in spite of the presence of oxygen vacancies characterized by a Raman band at 560 cm^{-1}. This effect is also observed after the addition of zirconium ions in the fluorite structure, although Zr atoms significantly improve thermal resistance to sintering. Neodymium cations in the valence state +III slightly inhibit oxygen mobility even though the structure is non-stoichiometric. This behaviour contrasts with that of praseodymium-doped ceria. Simultaneously at the Pr^{III} and Pr^{IV} valence state, Pr ions are able to promote oxygen mobility in the bulk starting at 500 K, with oxygen vacancies pre-existing at room temperature.

References

[1] A. Trovarelli, Structural properties and nonstoichiometric behavior of CeO_2, in: A. Trovarelli (Ed.), Catalysis by Ceria and Related Materials, Catalysis Science Series, Imperial College Press, 2002, p. 2 (Chapter 2).
[2] A. Trovarelli, Catal. Rev. Sci. Eng. 38 (1996) 439.
[3] J. Kaspar, P. Fornasiero, M. Graziani, Catal. Today 50 (1999) 285.
[4] M. Thammachart, V. Meeyo, T. Risksomboon, S. Osuwann, Catal. Today 68 (2001) 53.
[5] A. Cabana, J.A. Darr, E. Lester, M. Poliakoff, J. Mater. Chem. 11 (2001) 561.
[6] E. Rohart, O. Larcher, C. Hédouin, M. Allain, P. Macaudiére, SAE Int. Pape 1 (2001) 1274.
[7] J.-G. Li, T. Ikegami, T. Mori, Acta Mater. 52 (8) (2004) 2221.
[8] J.-G. Li, T. Ikegami, Y. Wang, T. Mori, J. Am. Ceram. Soc. 86 (6) (2003) 915.
[9] J.-G. Li, T. Ikegami, Y. Wang, T. Mori, J. Solid State Chem. 168 (1) (2002) 52.
[10] J.-G. Li, T. Ikegami, T. Mori, T. Wada, Chem. Mater. 13 (9) (2001) 13.
[11] P. Shuk, M. Greenblatt, M. Croft, J. Alloys Compd. 303 (2000) 465.
[12] S. Rossignol, C. Descorme, C. Kappenstein, D. Duprez, J. Mater. Chem. 11 (2001) 2587.
[13] C. Peng, Y. Wang, K. Jiang, B.Q. Bin, H.W. Liang, J. Feng, J. Meng, J. Alloys Compd. 349 (2000) 273.
[14] L. Li, X. Li, G. Li, H. Inimota, J. Mater. Res. 16 (11) (2001) 3207.
[15] W. Chun, G.W. Graham, J.A. Lupescu, R.W. McCabe, M.M. Koranne, R. Brezny, Catal. Lett. 106 (3–4) (2006) 95.
[16] W. Huang, P. Shuk, M. Greenblatt, Solid State Ion. 113 (1998) 305.
[17] S. Rossignol, D. Mesnard, F. Gerard, C. Kappenstein, D. Duprez, J. Mater. Chem. 13 (2003) 3017.
[18] C. Lamonier, G. Wrobel, J.P. Bonnelle, J. Mater. Chem. 4 (1994) 1927.
[19] F. Sadi, D. Duprez, F. Gérard, A. Miloudi, J. Cata 26 (2003) 226.
[20] S. Wang, W. Wang, J. Zuo, Y. Qian, Mater. Chem. Phys. 68 (2001) 246.
[21] S. Zha, Q. Fu, Y. Lang, C. Xia, G. Meng, Mater. Lett. 47 (2001) 351.
[22] S. Rossignol, F. Gérard, D. Duprez, J. Mater. Chem. 7 (1999) 1615.
[23] T. Biljan, S. Roncevic, Z. Meic, K. Kovac, Chem. Phys. Lett. 395 (2004) 246.
[24] A.M. Heyns, K.J. Range, J. Raman Spectroscopy 25 (1994) 855.
[25] A. Minesshige, T. Taji, Y. Muroi, M. Kobune, S. Fujii, N. Nishi, M. Inaba, Z. Ogumi, Solid State Ion. 135 (2000) 481.
[26] P. Fornasiero, A. Speghini, R. Di Monte, M. Bettinelli, J. Kaspar, A. Bigotto, V. Sergo, M. Graziani, Chem. Mater. 16 (10) (2004) 1938.
[27] H.C. Yao, Y.F. Yu Yao, J. Catal. 86 (1984) 254.
[28] P. Fornasiero, R. Di Monte, G. Ranga Rao, J. Kašpar, S. Meriani, A. Trovarelli, M. Graziani, J. Catal. 151 (1995) 168.
[29] D. Duprez, C. Descorme, Oxygen storage/Redox capacity and related phenomena on ceria-based catalysts, in: A. Trovarelli (Ed.), Catalysis by Ceria and Related Materials, Catalysis Science Series, Imperial College Press, 2002, pp. 243–280 (Chapter 7).
[30] M. Boaro, F. Giordano, S. Recchia, V. Dal Santo, M. Giona, A. Trovarelli, Appl. Catal. B 52 (2004) 225.
[31] N. Hickey, P. Fornasiero, R. Di. Monte, J. Kaspar, M. Graziani, G. Dolcetti, Catal. Lett. 72 (1) (2001) 45.
[32] R. Di. Monte, J. Kaspar, Top. Catal. 28 (1) (2004) 47.
[33] M. Ozawa, M. Kimura, A. Isogai, J. Alloys Compd. 193 (1993) 73.
[34] C. Binet, M. Daturi, J.C. Lavalley, Catal. Today 50 (1999) 207.
[35] D.-J. Kim, J. Am. Ceram. Soc. 72 (1989) 1415.
[36] M. Mogensen, Ceria-base electrodes, in: A. Trovarelli (Ed.), Catalysis by Ceria and Related Materials, Catalysis Science Series, Imperial College Press, 2002, pp. 453–481 (Chapter 15).
[37] S.J. Hong, A.V. Virkar, J. Am. Ceram. Soc. 78 (1995) 433.